Supplement of Nat. Hazards Earth Syst. Sci., 26, 675–701, 2026
https://doi.org/10.5194/nhess-26-675-2026-supplement

Natural Hazards and Earth System Sciences
Open Access
EGU

Supplement of

Flood risks to the financial stability of residential mortgage borrowers: an integrated modeling approach

Kieran P. Fitzmaurice et al.

Correspondence to: Kieran P. Fitzmaurice (kieranf@ad.unc.edu)

Table of contents

Supplementary methods

Section S1. Processing of NFIP claim and policy records.

The insurance status of each property at the time of included flood events is determined based on address-level records of NFIP policies and filed claims provided by FEMA Region IV. These records were geocoded to specific properties using the Google Maps Geocoding API and the provided address (Google Maps Platform, 2022). Overall, 78% of claim and 85% of policy records were successfully matched to properties using a 30-meter maximum distance tolerance. We determined the start and end dates of included flood events based on daily counts of NFIP claims across the state. We further limited the spatial extent of each event by excluding records from counties with less than 20 NFIP claims filed between the previously determined start and end dates (Fig. S1). The final dataset consisted of 39,702 claims and 142,092 policy records from seven unique flood events, representing 53% of all NFIP claims filed in North Carolina during the 1996-2019 period (Table S2).

Not all NFIP policies were included in the address-level dataset provided by FEMA. When compared against publicly available sources of data such as the OpenFEMA NFIP Redacted Policies Dataset (FEMA, 2025), it becomes clear that the address-level policy data only represents a subset of the total policy base in force: this ranged from 21% during Hurricane Florence to 56% during Hurricane Irene (Table S2). This issue was specific to policies, which are used to determine the location of "absence" points within the machine learning framework (model I, Sect. 3.3), and did not appear to affect claims, which are used to determine "presence" points and exhibited good agreement with OpenFEMA data. To adjust for the potential effect of missing absence points on model predictions, we randomly selected structures within the study area as "pseudo-absence" points to be included as examples within the training data. These points were selected using a geographically stratified sampling scheme such that the number of absence points within small geographic units matched the totals implied by auxiliary sources of data. For post-2009 flood events, census tract-level policy enrollment data published by OpenFEMA was used to determine the target number of absence points within each geographic unit, which were defined based on the intersection of census tract and SFHA polygons. For events occurring prior to 2009 (the earliest date for which OpenFEMA policy data is available), anonymized zip code-level data on NFIP policy enrollment was used to determine the target number of absence points, with

geographic units defined based on the intersection of Census Bureau Zip Code Tabulation Areas (ZCTAs) and SFHA polygons. Within each geographic unit, the number of sampled pseudo-absence points (N_{PA}) was determined as follows:

$$N_{PA,i} = \max\left(N_{B,i}\ ,\ N_{A,i}^{Auxiliary} - N_{A,i}^{Address}\right) \quad \text{(Eq. S1)}$$

where i is a subscript denoting a specific geographic unit, N_B is the number of buildings not previously matched to an address-level NFIP claim or policy, $N_A^{Auxiliary}$ is the target number of absence points implied by auxiliary data sources, and $N_A^{Address}$ is the number of absence points implied by the address-level NFIP claim and policy data. The number of presence, absence, and pseudo-absence points for each evaluated event are listed in Table S2.

Section S2. Modeling the space-time covariance structure of property values.

In the second step of our property value estimation procedure, the spatiotemporal component $\hat{Z}(\boldsymbol{s_i}, t)$ is estimated via space-time interpolation of hedonic residuals using the simple lognormal kriging method (Chilès and Delfiner, 2012, p.150, 193). This method requires the specification of a covariance function describing the structure of spatial and temporal autocorrelation in home prices; to this end, we constructed a sample variogram from spatially and temporally lagged pairs of hedonic residuals using the Mathéron variogram estimator (Chilès and Delfiner, 2012, p.37; Mathéron, 1965). Next, we fit the following product-sum space-time covariance model to the sample variogram (Chilès and Delfiner, 2012, p.114; Iaco et al., 2001):

$$C(h_s, h_t) = c_0 + k_1 C_s(h_s) C_t(h_t) + k_2 C_s(h_s) \quad \text{(Eq. S2)}$$

where h_s and h_t are the spatial and temporal distance (respectively) between a given pair of hedonic residuals and $C_s(h_s)$ and $C_t(h_t)$ are respectively the spatial and temporal components of the space-time covariance function. The parameters c_0, k_1, and k_2 were estimated via least squares from the sample variogram. The purely spatial component $C_s(h_s)$ was modeled as a spherical covariance function with a spatial range estimated via least squares; the purely temporal component $C_t(h_t)$ was modeled as an exponential covariance function with a temporal range of 365 days (Chilès and Delfiner, 2012, p.84).

Section S3. Variance-based sensitivity analysis of uncertain model parameters.

To better understand the contribution of key model parameters to uncertainty in the post-flood financial conditions of mortgage borrowers, we conducted a variance-based sensitivity analysis using the method of Sobol' (Sobol′, 1993, 2001). This approach decomposes the variance of model outputs into terms that can be attributed to uncertain input parameters and their interactions. In our analysis, we focused on uncertainty in the following components of our integrated modeling framework: damage costs (model I), property values (model II), and borrower incomes (model IV) at the time of their flood exposure. These parameters were selected because they represent the primary drivers of flood-related credit constraints and are used directly within the calculation of combined loan-to-value (ACLTV) and debt-to-income (ADTI) ratios for flood-exposed borrowers. When examining how uncertainty in these input parameters contributes to uncertainty in model outputs, we focused on the following outcomes of interest: (1) the outcome of a borrower being collateral constrained (ACLTV > 100%), (2) the outcome of a borrower being income constrained (ADTI > 45%), (3) the outcome of being constrained by both measures (ACLTV > 100% and ADTI > 45%), and (4) the outcome of being constrained by either measure (ACLTV > 100% or ADTI > 45%). Because these model inputs and outcomes of interest are defined at the level of individual borrowers, sensitivity indices were calculated separately for each borrower based on their simulated financial conditions at the time of flood exposure.

Damage costs were assumed to follow a lognormal distribution with a mean equal to the model-predicted cost at each property location and variance estimated from cross-validation residuals using the conditional variance estimator of Fan and Yao (1998). This approach allows the amount of variance in damage costs to vary as a smooth function of the mean estimate, reflecting the higher uncertainty in total costs for properties predicted to have severe damage (Fig. S20). These mean-variance relationships were fit separately for each of the seven evaluated flood events.

Property values were assumed to follow a lognormal distribution with a mean equal to the model-predicted property value at each location and variance estimated via space-time interpolation of hedonic residuals using the simple lognormal kriging method (Chilès and Delfiner, 2012, p.150, 193). Because the kriging method provides an estimate of the error variance at each prediction point, it is well-suited for characterizing the uncertainty in property value estimates.

Borrower income was assumed to evolve over time as a stochastic process following geometric Brownian motion (GBM). GBM is frequently used to model the evolution of asset prices and other financial quantities that are assumed to be

lognormally distributed (Hull, 2018). For each borrower, the initial conditions of this process were specified based on their simulated income at the time of mortgage origination (I_{t_0}). In timepoints following origination, their income is modeled according to GBM as a lognormal distribution with the following mean and variance:

$$E[I_t] = I_{t_0} e^{\mu(t-t_0)} \quad \text{(Eq. S3)}$$

$$V[I_t] = I_{t_0}^2 e^{2\mu(t-t_0)} \left(e^{\sigma^2(t-t_0)} - 1\right) \quad \text{(Eq. S4)}$$

where μ and σ represent the expected annual growth and annualized volatility of borrower income respectively. For each borrower, μ was calculated based on the average continuously-compounded growth in per-capita income in their county of residence since the time of origination (BEA, 2023). The value of σ was fixed at 7% per year; this assumption is loosely based on Figure 3 of Dynan et al. (2012), who observed that the standard deviation of two-year changes in income for households in the middle 50% of the income distribution was approximately 10% during the 1971-2008 period (10% / $\sqrt{2} \approx$ 7%).

First order and total effect Sobol' indices were calculated using the estimator of Saltelli et al. (2010) implemented by the SciPy Python library (Virtanen et al., 2020). The first order index (S_i) reflects the share of output variability that can be directly explained by a given parameter in isolation while ignoring interaction effects with other inputs. The total effect index (S_{T_i}) reflects the share of output variability that a given parameter contributes to either directly or through its interactions with other variables. For each borrower, our calculation procedure results in a total of 12 index pairs (3 input parameters × 4 outcomes of interest). To evaluate the relative contribution different parameters to uncertainty in model outputs, parameters were ranked individually for each borrower based on the total effect index, and the frequency of different ranking orders summarized across the simulated population of mortgage borrowers (Table S8). Similarly, population-averaged index values were computed by weighing the Sobol' indices of individual borrowers by the variance in their outcomes of interest:

$$\overline{S_i} = \frac{\sum_{k=1}^{N} V_k S_{ik}}{\sum_{k=1}^{N} V_k} \quad \text{(Eq. S5)}$$

$$\overline{S_{T_i}} = \frac{\sum_{k=1}^{N} V_k S_{T_{ik}}}{\sum_{k=1}^{N} V_k} \quad \text{(Eq. S6)}$$

In Eq. S5 and Eq. S6, V_k denotes the variance of the outcome of interest for borrower k, while $\overline{S_i}$ and $\overline{S_{T_i}}$ denote the weighted average first order and total effect indices (respectively) of parameter i across the population. Weighted average index values for different parameter-outcome combinations are displayed in Fig. S21.

Supplementary tables

Table S1. Variables and data sources used within the modeling framework.

Sub-Model / Variable Name	Variable Type	Spatial Resolution	Temporal Resolution	Source
Flood damage (model I)				
SFHA status	Binary	Property	--	FEMA
First floor elevation	Continuous	Property	--	NCEM
Year built	Discrete	Property	--	NCEM
Tax-assessed value	Continuous	Property	--	NCEM
Heated square footage	Continuous	Property	--	NCEM
Occupancy type	Categorical	Property	--	NCEM
Foundation type	Categorical	Property	--	NCEM
HUC6 watershed	Categorical	Property	--	NHD
Maximum 3-day precipitation during event	Continuous	1 km raster	Daily	Daymet V4
Distance to coast	Continuous	30 m raster	--	NHD
Distance to nearest stream	Continuous	30 m raster	--	NHD
Height above nearest drainage	Continuous	30 m raster	--	NHD, NED
Topographic wetness index	Continuous	30 m raster	--	NHD, NED
Soil hydraulic conductivity	Continuous	30 m raster	--	NHD
Impervious surface percentage	Continuous	30 m raster	--	NLCD
Average slope	Continuous	HUC12 subbasin	--	NED
Elevation	Continuous	30 m raster	--	NED
Property value (model II)				
Heated square footage	Continuous	Property	--	NCEM
Parcel square footage	Continuous	Property	--	NC OneMap
Year built	Discrete	Property	--	NCEM
Tax-assessed value	Continuous	Property	--	NCEM
Median household income in 2019	Continuous	Census tract	--	ACS
Home price index	Continuous	County	Annual	FHA
25^{th} percentile of newly originated mortgage loan amounts	Continuous	Census tract	Annual	HMDA
50^{th} percentile of newly originated mortgage loan amounts	Continuous	Census tract	Annual	HMDA
75^{th} percentile of newly originated mortgage loan amounts	Continuous	Census tract	Annual	HDMA
Mortgage repayment (model III)				
Loan amount	Continuous	Census tract	Annual	HMDA
Borrower income at origination	Continuous	Census tract	Annual	HMDA
LTV at origination	Distribution	State	Annual	FNMA, FHLMC
DTI at origination	Distribution	State	Annual	FNMA, FHLMC
Interest rate spread	Distribution	State	Annual	FNMA, FHLMC

SFHA: Special Flood Hazard Area. FEMA: Federal Emergency Management Agency. NCEM: NC Emergency Management. HUC: Hydrologic Unit Code. NHD: National Hydrography Dataset. NED: National Elevation Dataset. NLCD: National Land Cover Database. ACS: American Community Survey. FHA: Federal Housing Administration. HMDA: Home Mortgage Disclosure Act. LTV: Loan-to-value ratio. DTI: Debt-to-income ratio. FNMA: Fannie Mae. FHLMC: Freddie Mac

Table S2. Number of included NFIP records and presence-absence points by flood event.

Flood event	NFIP claims in included counties	NFIP policies-in-force in included counties by data source			Presence points	Absence points	Pseudo-absence points
		Address-level data	Tract-level data	Zip code-level data			
Fran (1996)	5,820	5,382	--	65,050	5,474	4,889	43,308
Bonnie (1998)	1,764	10,258	--	73,723	1,669	9,297	49,515
Floyd (1999)	6,684	7,906	--	85,019	6,266	7,285	55,192
Isabel (2003)	3,631	5,914	--	56,651	3,424	5,227	39,369
Irene (2011)	6,292	54,071	96,390	--	6,063	49,141	42,517
Matthew (2016)	4,127	38,620	102,463	--	3,955	36,588	64,110
Florence (2018)	11,384	19,941	95,801	--	11,057	17,123	63,371

Table S3. Cross-validation performance of the random forest model by event.

CV method / Performance metric	Value by event						
	Fran (1996)	**Bonnie (1998)**	**Floyd (1999)**	**Isabel (2003)**	**Irene (2011)**	**Matthew (2016)**	**Florence (2018)**
Random CV							
ROC-AUC	0.95	0.87	0.86	0.94	0.94	0.92	0.91
Accuracy	0.92	0.97	0.92	0.95	0.95	0.97	0.92
Sensitivity	0.31	0.15	0.12	0.39	0.23	0.22	0.42
Specificity	0.99	1.00	0.99	0.99	0.99	1.00	0.98
Precision	0.75	0.54	0.70	0.71	0.72	0.76	0.78
R^2 score[a]	0.07	-0.01	0.05	0.07	0.10	0.23	0.39
R^2 score among true positives	0.06	0.03	0.25	0.13	0.12	0.41	0.45
Spatially aggregated R^2 score[b]	0.87	0.64	0.54	0.63	0.52	0.55	0.93
Spatial block CV							
ROC-AUC	0.87	0.79	0.79	0.84	0.92	0.86	0.86
Accuracy	0.90	0.97	0.91	0.93	0.94	0.96	0.91
Sensitivity	0.11	0.00	0.01	0.10	0.20	0.12	0.33
Specificity	0.99	1.00	1.00	1.00	0.99	1.00	0.99
Precision	0.61	0.21	0.69	0.66	0.66	0.63	0.75
R^2 score[a]	-0.02	-0.01	-0.01	-0.01	0.06	0.06	0.25
R^2 score among true positives	0.01	-0.17	-0.02	-0.02	0.02	0.38	0.31
Spatially aggregated R^2 score[b]	0.76	0.02	-0.06	0.05	0.30	0.19	0.80

CV: Cross-validation. ROC: Receiver operating characteristic. AUC: Area under curve.

[a]Unlike binary classification performance metrics (e.g., accuracy), which are calculated based on the predicted presence or absence of flood damage, the R^2 score is calculated based on the dollar amount of damage predicted at each property.

[b]Spatially aggregated R^2 scores are calculated by comparing predicted and observed damage to NFIP-insured properties after aggregating damages across 5 km square grid cells.

Table S4. Confusion matrices of the random forest model by event.

CV method / Classification outcome	Frequency of classification outcomes by event, n (%)						
	Fran (1996)	**Bonnie (1998)**	**Floyd (1999)**	**Isabel (2003)**	**Irene (2011)**	**Matthew (2016)**	**Florence (2018)**
Random CV							
TP	1,672 (3.1%)	246 (0.4%)	765 (1.1%)	1,335 (2.8%)	1,373 (1.4%)	851 (0.8%)	4,600 (5.0%)
TN	47,637 (88.8%)	58,605 (96.9%)	62,146 (90.4%)	44,054 (91.7%)	91,122 (93.2%)	100,427 (96.0%)	79,226 (86.5%)
FP	560 (1.0%)	207 (0.3%)	331 (0.5%)	542 (1.1%)	536 (0.5%)	271 (0.3%)	1,268 (1.4%)
FN	3,802 (7.1%)	1,423 (2.4%)	5,501 (8.0%)	2,089 (4.4%)	4,690 (4.8%)	3,104 (3.0%)	6,457 (7.1%)
Total	53,671 (100.0%)	60,481 (100.0%)	68,743 (100.0%)	48,020 (100.0%)	97,721 (100.0%)	104,653 (100.0%)	91,551 (100.0%)
Spatial block CV							
TP	597 (1.1%)	8 (0.0%)	75 (0.1%)	328 (0.7%)	1,213 (1.2%)	455 (0.4%)	3,680 (4.0%)
TN	47,816 (89.1%)	58,782 (97.2%)	62,444 (90.8%)	44,428 (92.5%)	91,032 (93.2%)	100,430 (96.0%)	79,291 (86.6%)
FP	381 (0.7%)	30 (0.0%)	33 (0.0%)	168 (0.3%)	626 (0.6%)	268 (0.3%)	1,203 (1.3%)
FN	4,877 (9.1%)	1,661 (2.7%)	6,191 (9.0%)	3,096 (6.4%)	4,850 (5.0%)	3,500 (3.3%)	7,377 (8.1%)
Total	53,671 (100.0%)	60,481 (100.0%)	68,743 (100.0%)	48,020 (100.0%)	97,721 (100.0%)	104,653 (100.0%)	91,551 (100.0%)

SFHA: Special Flood Hazard Area. CV: Cross-validation. TP: True positives. TN: True negatives. FP: False positives. FN: False negatives

Table S5. Cox proportional hazards regression analysis of mortgage prepayment rates.

Loan purpose / Term	Interest rate benchmark used in rate spread calculation	Number of loan-month observations	Number of repayment events	Rate spread regression coefficient (95% CI)	Hazard ratio (95% CI)
Home purchase					
30-year	MORTGAGE30US	38,829,210	262,832	0.48 (0.48–0.49)	1.62 (1.61–1.63)
Refinance					
30-year	MORTGAGE30US	46,395,034	299,819	0.40 (0.39–0.40)	1.49 (1.48–1.49)
15-year	MORTGAGE15US	29,383,696	171,555	0.27 (0.27–0.28)	1.31 (1.31–1.32)

MORTGAGE30US: 30-year fixed rate mortgage average in the United States (Freddie Mac, 2016b). MORTGAGE15US: 15-year fixed rate mortgage average in the United States (Freddie Mac, 2016a). CI: Confidence interval.

Table S6. Conceptual model of mortgage borrower finances.

Line item[a]	Corresponding variable in model IV	Units
Household balance sheet		
Assets		
Primary residence	P_t	USD (nominal)
Secondary and rental properties	Not modeled	--
Liquid savings	Not modeled	--
Retirement and investment accounts	Not modeled	--
Vehicles and other personal property	Not modeled	--
Liabilities		
Primary mortgage	$B_{M,t}$	USD (nominal)
Home repair loans[b]	$B_{R,i,t}$	USD (nominal)
Mortgages on other properties	Not modeled	--
Auto loans	Not modeled	--
Student loans	Not modeled	--
Credit cards	Not modeled	--
Unpaid bills and other debt	Not modeled	--
Household cashflows		
Cash inflows		
Stable and predictable income[c]	I_t	USD per month
Fluctuating and variable income[c]	Not modeled	--
Post-disaster aid	Not modeled	--
Cash outflows		
Primary mortgage payment	c_M	USD per month
Repair loan payments[b]	$c_{R,i}$	USD per month
Other recurring debt obligations[d]	c_{NM}	USD per month
Taxes and insurance[e]	Not modeled	--

USD: United States dollars.

[a]The entries listed within this table represent a non-exhaustive list of common household budget items.

[b]Uninsured borrowers are assumed to finance flood-related repairs through home equity-based borrowing.

[c]Borrower income is initialized at origination and assumed to evolve deterministically over time according to county-level trends in personal income growth. We did not model exogenous shocks to household income or changes in employment status.

[d]Includes payments on sources of debt which were not explicitly modeled (e.g., auto loans, credit cards) but which nevertheless affect a borrower's DTI ratio. These obligations are assumed to remain constant over time.

[e]We did not model housing expenses associated with property taxes, homeowners' insurance, or flood insurance.

Table S7. Flood damage to properties within the study area by event and across comparative groups.

Stratification variable	Flooded properties, n (%)[a]	Flood damage cost, USD[b] (% repetitive)[c]	
		Insured	Uninsured
Flood event			
Fran (1996)	6,300 (0.15%)	185,915,000 (0%)	29,812,000 (0%)
Bonnie (1998)	2,100 (0.05%)	20,799,000 (71%)	5,001,000 (15%)
Floyd (1999)	20,500 (0.48%)	180,077,000 (35%)	720,058,000 (0%)
Isabel (2003)	7,200 (0.17%)	91,858,000 (11%)	95,831,000 (0%)
Irene (2011)	8,700 (0.20%)	159,240,000 (51%)	98,643,000 (33%)
Matthew (2016)	16,300 (0.38%)	174,265,000 (25%)	752,584,000 (1%)
Florence (2018)	23,900 (0.56%)	548,982,000 (51%)	892,383,000 (18%)
SFHA status			
SFHA	31,600 (21.93%)	1,092,714,000 (39%)	902,960,000 (17%)
Non-SFHA	35,600 (0.86%)	268,422,000 (23%)	1,691,353,000 (3%)
Proximity to coasts			
CAMA counties	33,000 (5.46%)	1,035,977,000 (39%)	725,479,000 (14%)
Non-CAMA counties	34,200 (0.92%)	325,160,000 (27%)	1,868,834,000 (5%)
Urban-rural classification			
Urban	32,700 (1.60%)	661,636,000 (39%)	1,406,678,000 (9%)
Rural	34,400 (1.52%)	699,501,000 (33%)	1,187,635,000 (6%)
Overall	67,200 (1.56%)	1,361,137,000 (36%)	2,594,313,000 (8%)

USD: United States dollars. SFHA: Special Flood Hazard Area. CAMA: Coastal Area Management Act.

[a]Percentages denote the share of all properties in a given category that were exposed to flooding.

[b]Monetary amounts are adjusted for inflation and expressed in 2020 United States dollars.

[c]Percentages denote the share of flood-related damage attributable to repetitive losses (i.e., damages occurring after a property's first exposure to flooding during the study period).

Table S8. Ranking uncertain parameters by their influence on borrower outcomes.

Outcome of interest / Parameter ranking[a]	Parameter ranking frequency[b] (%)		
	Property value	**Damage cost**	**Income**
Collateral constrained (ACLTV > 100%)			
1st most influential parameter	95.9	4.1	0.0
2nd most influential parameter	4.1	95.8	0.0
3rd most influential parameter	0.0	0.0	100.0
Income constrained (ADTI > 45%)			
1st most influential parameter	1.9[c]	58.3	39.9
2nd most influential parameter	0.4[c]	39.8	59.7
3rd most influential parameter	97.7	1.9	0.4
Constrained by both (ACLTV > 100% and ADTI > 45%)			
1st most influential parameter	14.8	70.6	14.7
2nd most influential parameter	12.6	22.8	64.5
3rd most influential parameter	72.6	6.6	20.8
Constrained by either (ACLTV > 100% or ADTI > 45%)			
1st most influential parameter	78.8	9.2	12.0
2nd most influential parameter	11.1	79.7	9.2
3rd most influential parameter	10.1	11.1	78.8

ACLTV: Adjusted combined loan-to-value ratio. ADTI: Adjusted debt-to-income ratio.

[a]For each borrower, uncertain parameters are ranked from most to least influential based on their Sobol' total effect index for the outcome of interest.

[b]Ranking frequencies reflect the share of flood-exposed borrowers for which a given parameter was found to be the *n*th most influential.

[c]In theory, property value should have no influence on the outcome of a borrower being income constrained. However, this parameter occasionally has a non-zero Sobol' total effect index due to numerical error in the calculation. This issue only occurs when the amount of variance in the outcome of interest is close to zero.

Supplementary figures

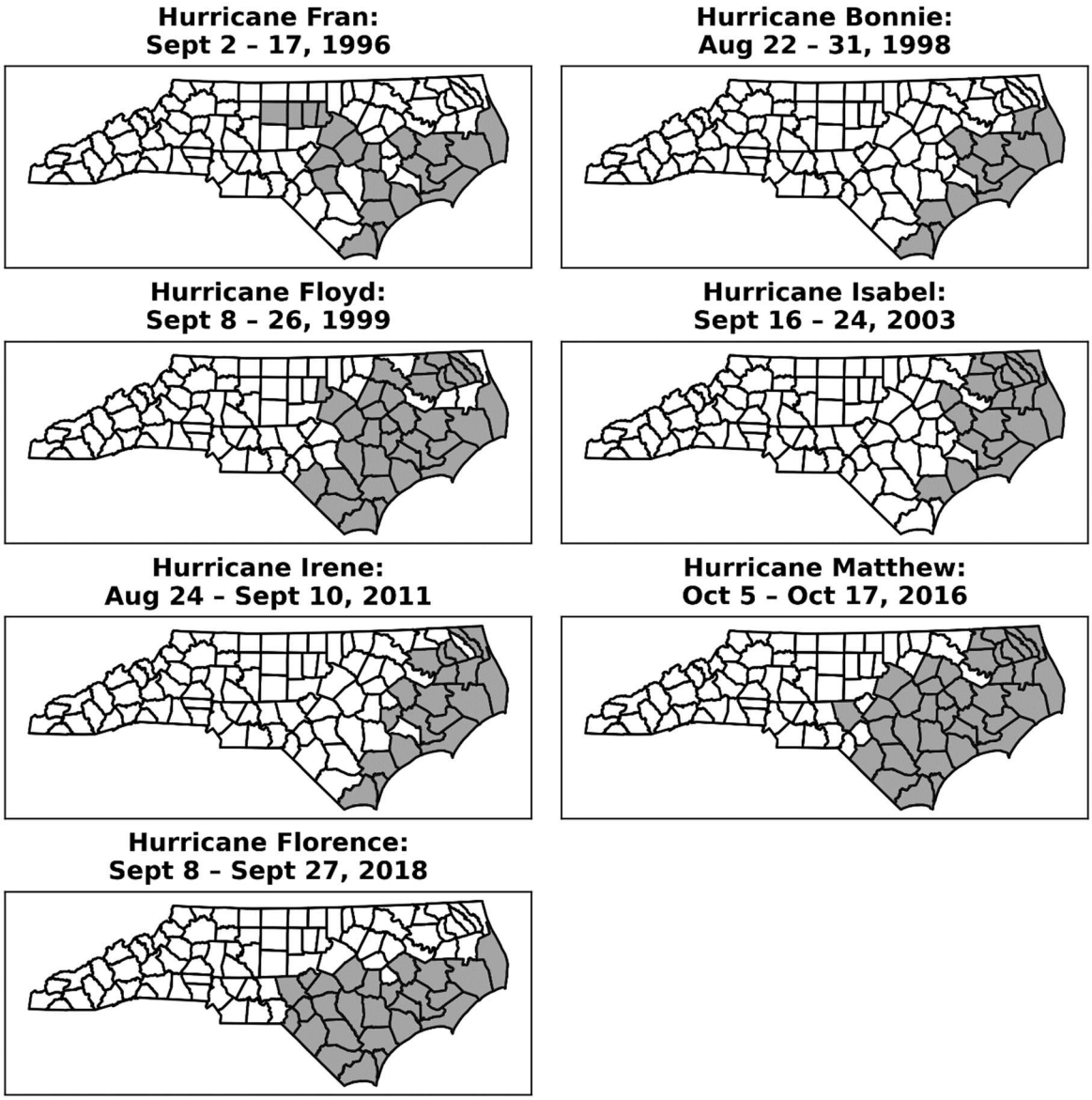

Figure S1. Spatial and temporal boundaries of included flood events.

Shaded regions denote counties included in the flood damage estimation model for each event. NFIP claims occurring in included counties during the listed date range are assumed to result from flood damage incurred during the named event. All counties included in an event must have at least 20 associated claims.

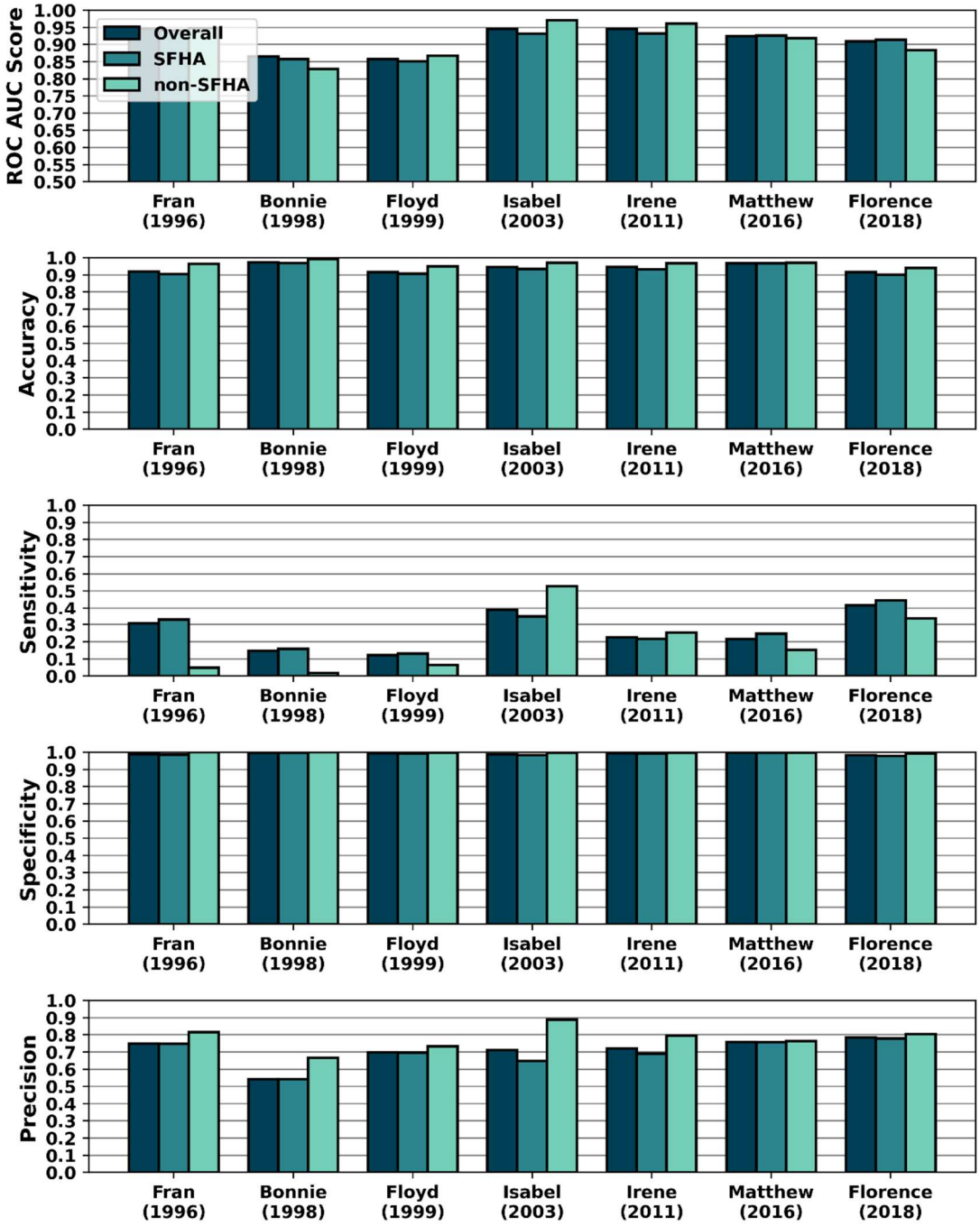

Figure S2. Cross-validation performance of the random forest model.

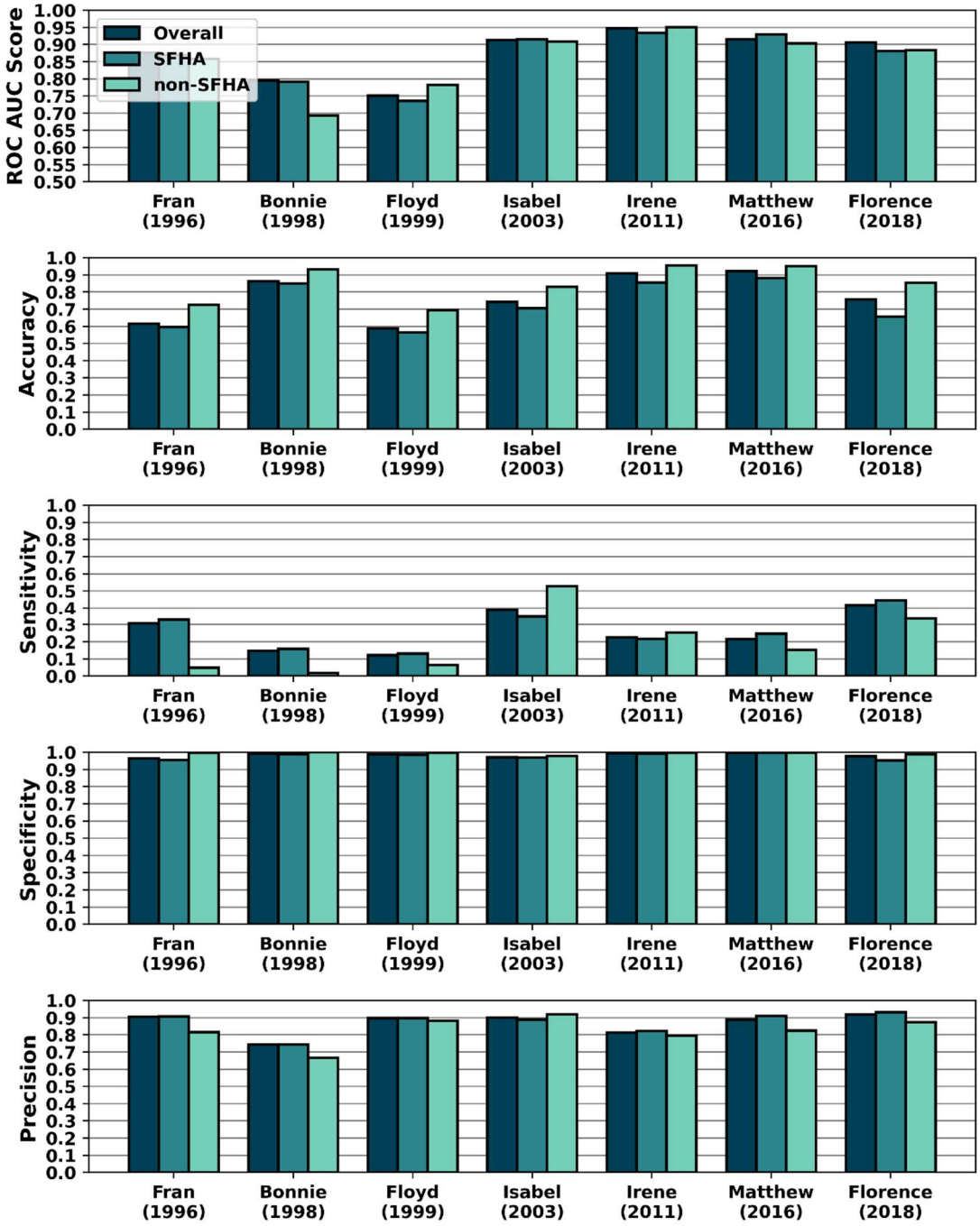

Figure S3. Cross-validation performance of the random forest model when pseudo-absences are excluded from the validation data.

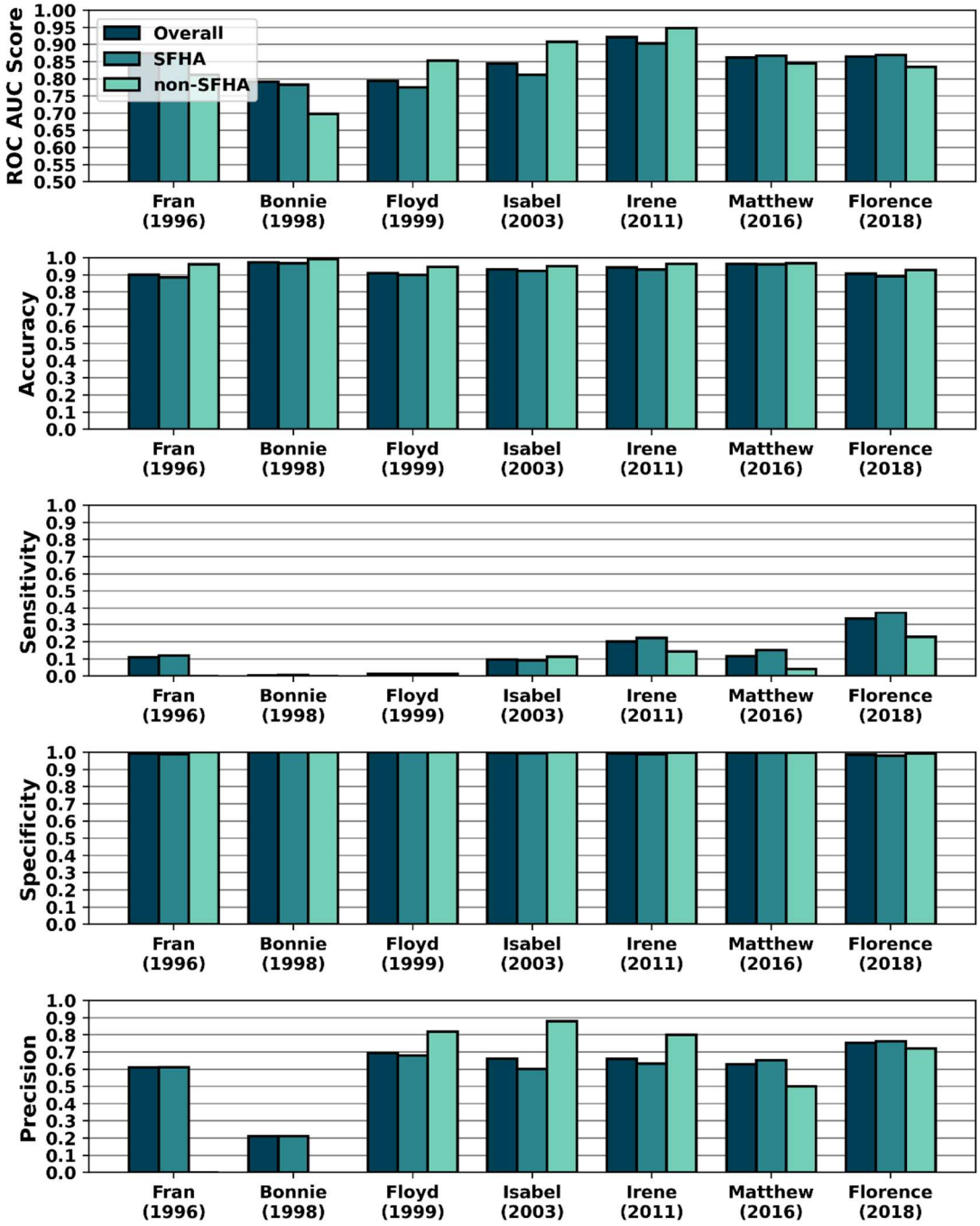

Figure S4. Spatial block cross-validation performance of the random forest model.

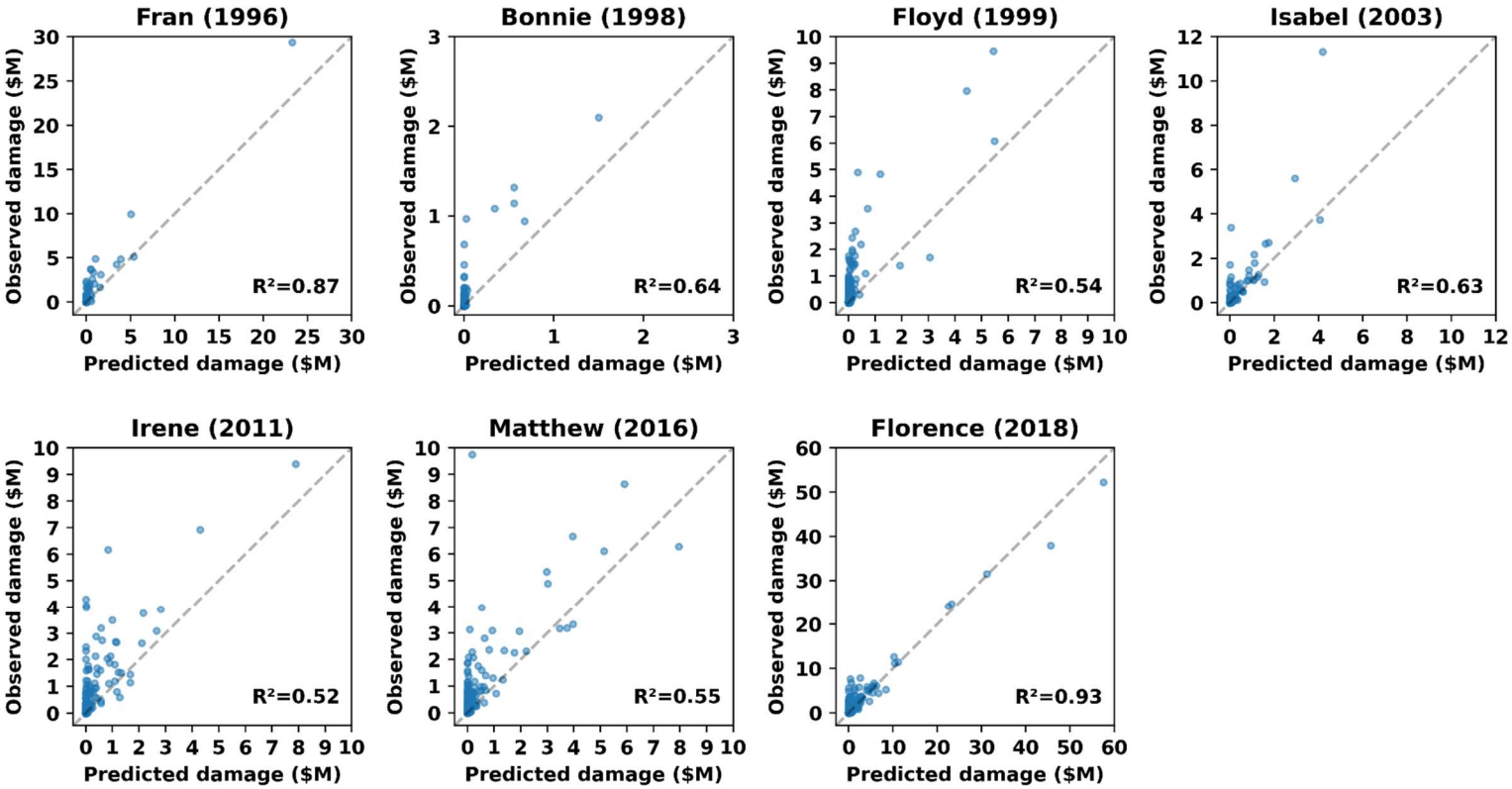

Figure S5. Cross-validation error of damage cost predictions after spatial aggregation.

In each panel, the y-axis represents observed damage among properties in the insured dataset, while the x-axis represents damage predicted by the random forest model in cross-validation. The x- and y-coordinates of each point are determined by aggregating predicted and observed damage to NFIP-insured properties across 5 km square grid cells.

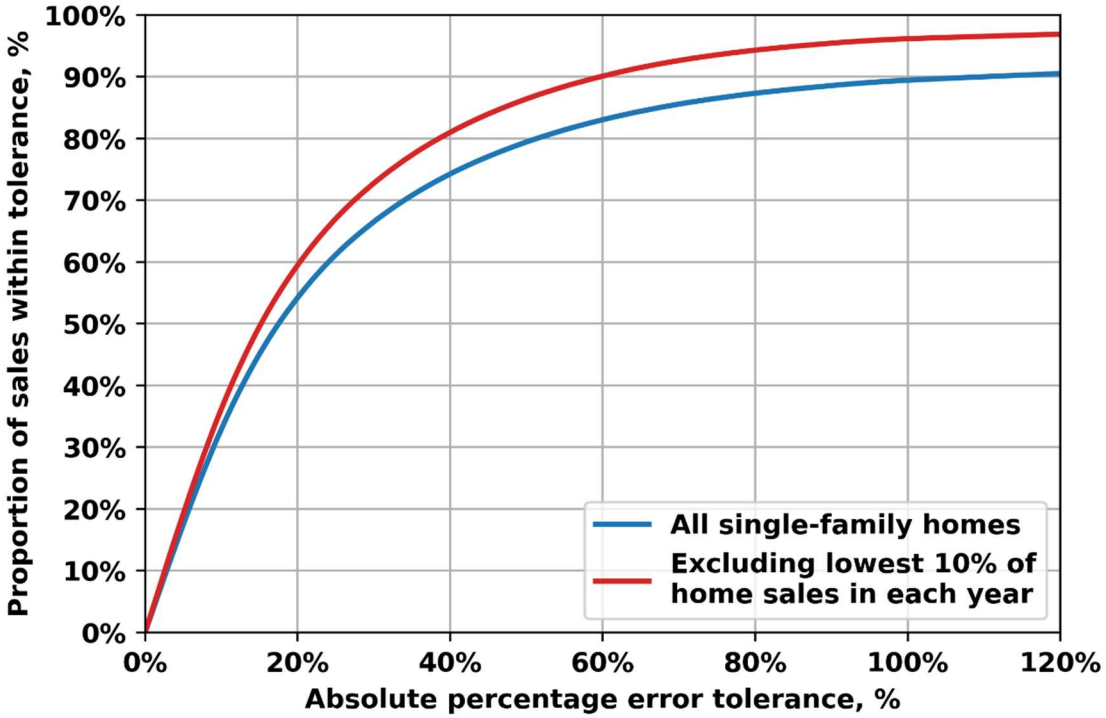

Figure S6. Empirical cumulative distribution function of property value model errors.

The absolute percentage error between the model-predicted and observed property sale price is plotted on the x-axis, while the proportion of cross validation predictions within a given error tolerance is plotted on the y-axis.

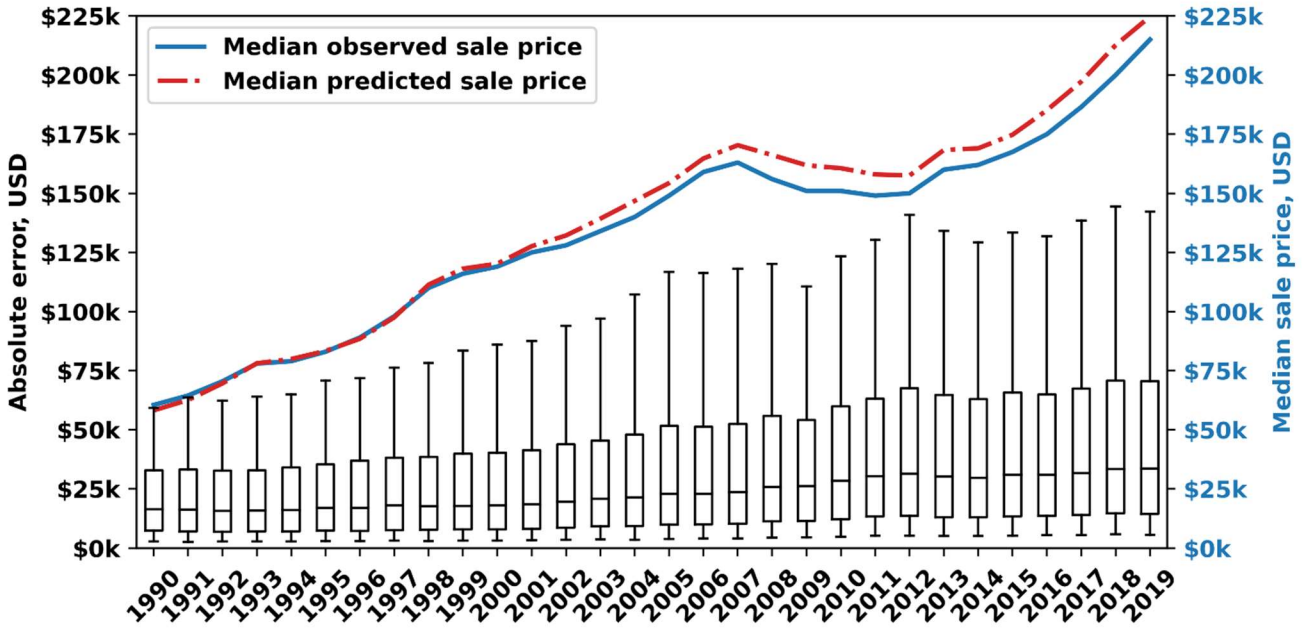

Figure S7. Property value model error by period.

The distribution of absolute error associated with cross-validation predictions for sales occurring in a given year are depicted by the black box-and-whisker plots. Whisker boundaries correspond to the 10th and 90th percentiles of absolute error. For comparison purposes, the median observed sale price of properties included in our sample in each year is depicted by the blue line, while the median predicted sale price is depicted by the red dashed line.

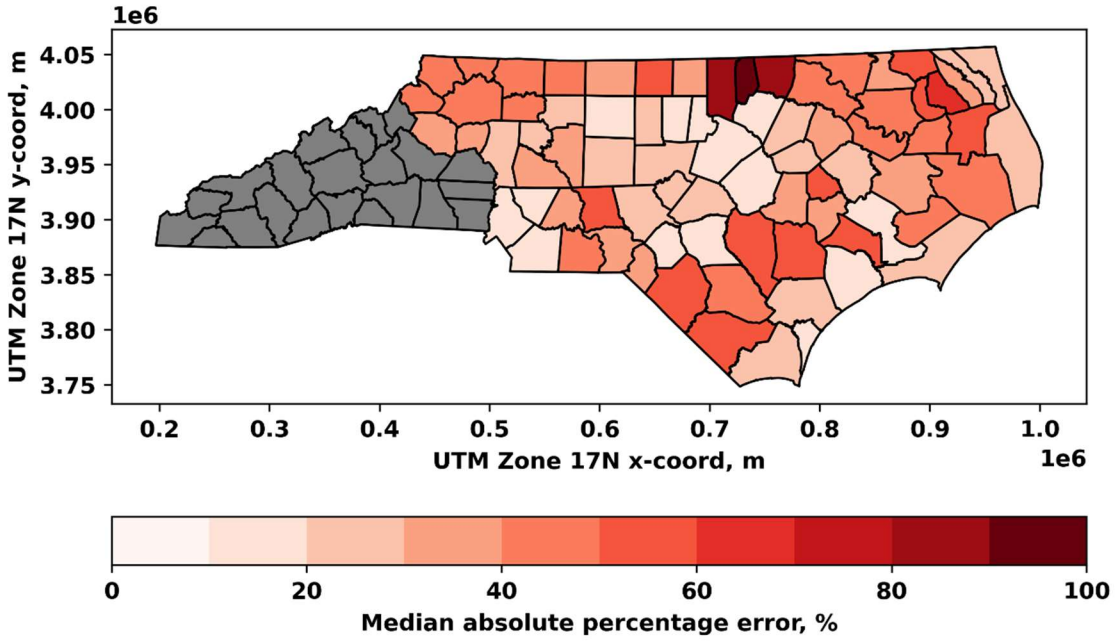

Figure S8. Median absolute percentage error of the property value model by county.

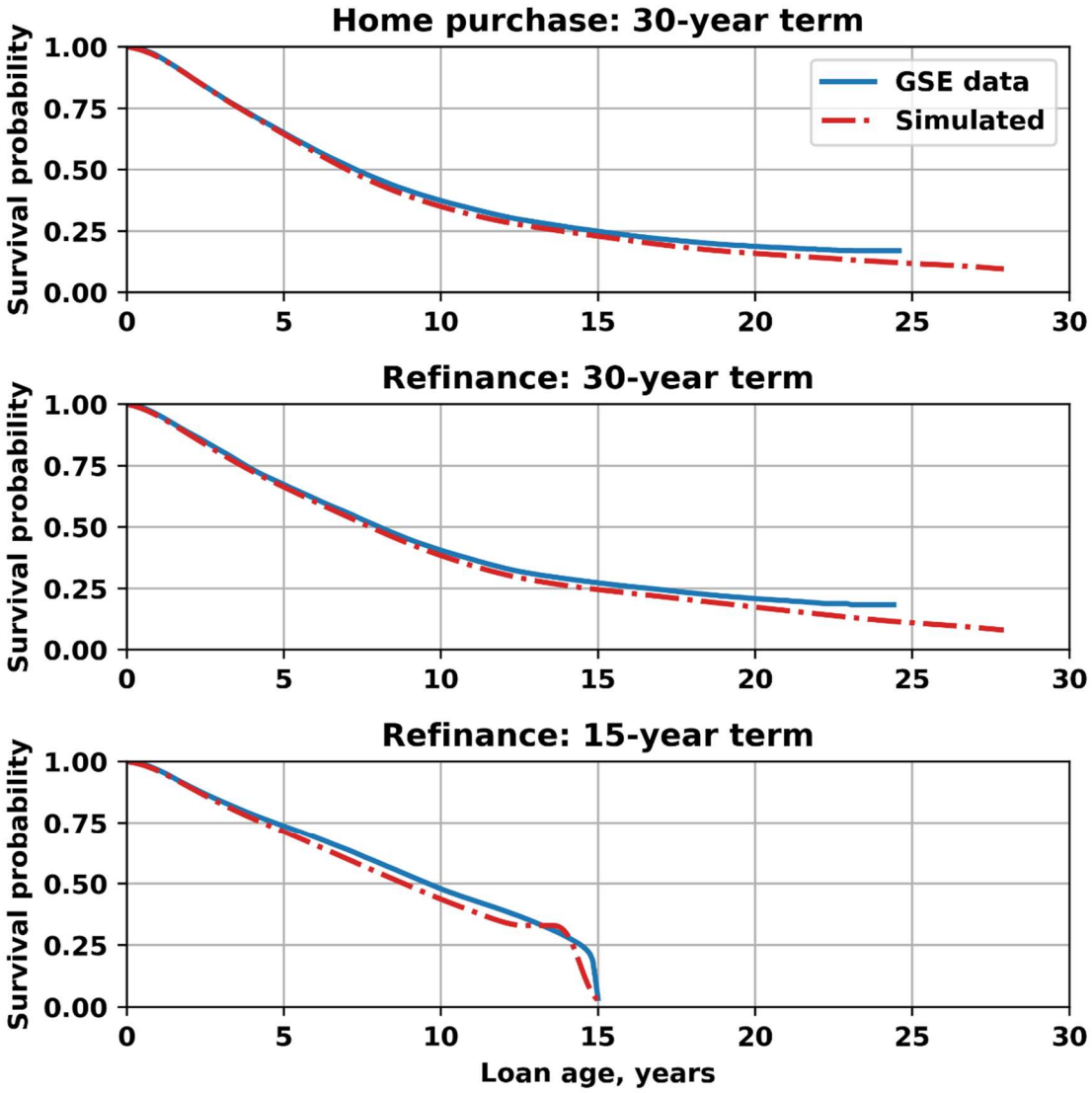

Figure S9. Simulated and empirically observed mortgage repayment profiles.

Survival curves for North Carolina mortgages purchased by the GSEs from 1999-2021 are represented by blue lines. Survival curves for simulated mortgage are denoted by red dashed lines. In both cases, survival curves were constructed using the Kaplan-Meier estimator and stratified by the loan purpose (home purchase or refinance) and loan term (30 or 15 years).

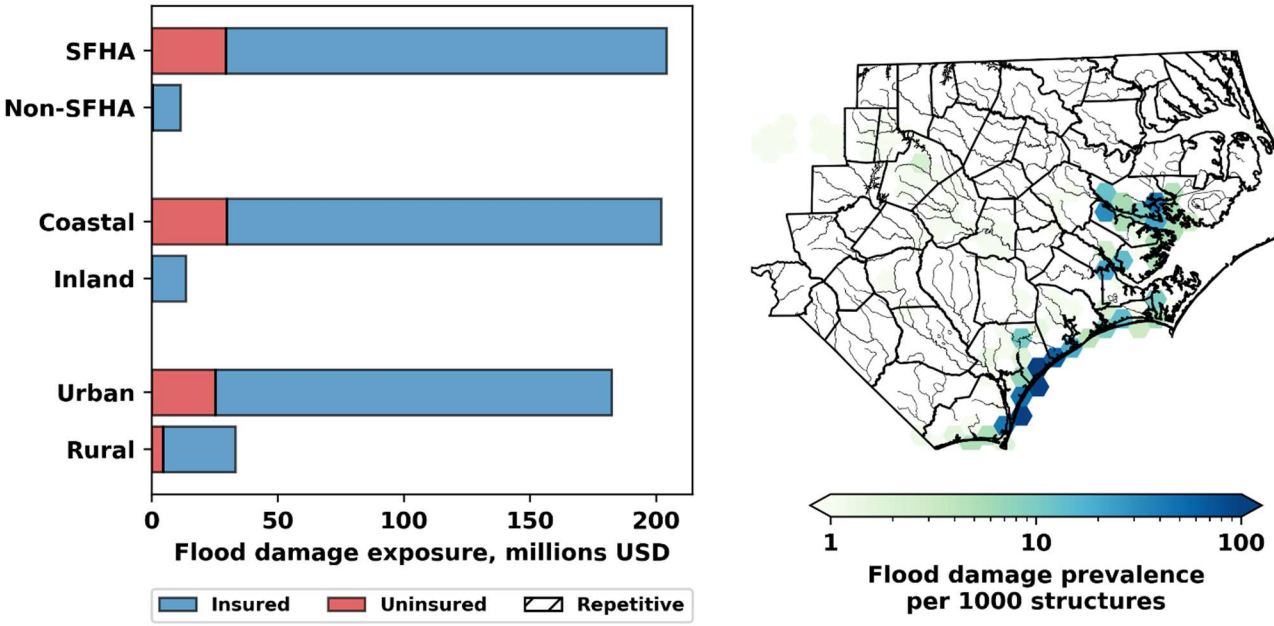

Figure S10. Prevalence and cost of flood damage during Hurricane Fran (1996).

The left panel depicts the aggregate cost of flood damage across comparative groups, while the right panel depicts the spatial distribution of flooded structures across a uniform 15 km hexagonal grid. Bars should only be compared within appropriate pairs (e.g., SFHA vs. non-SFHA) but not across pairs (e.g., SFHA vs. Coastal) as groups across pairs are not mutually exclusive. For display purposes, only counties that are members of the nine easternmost regional councils in North Carolina are shown.

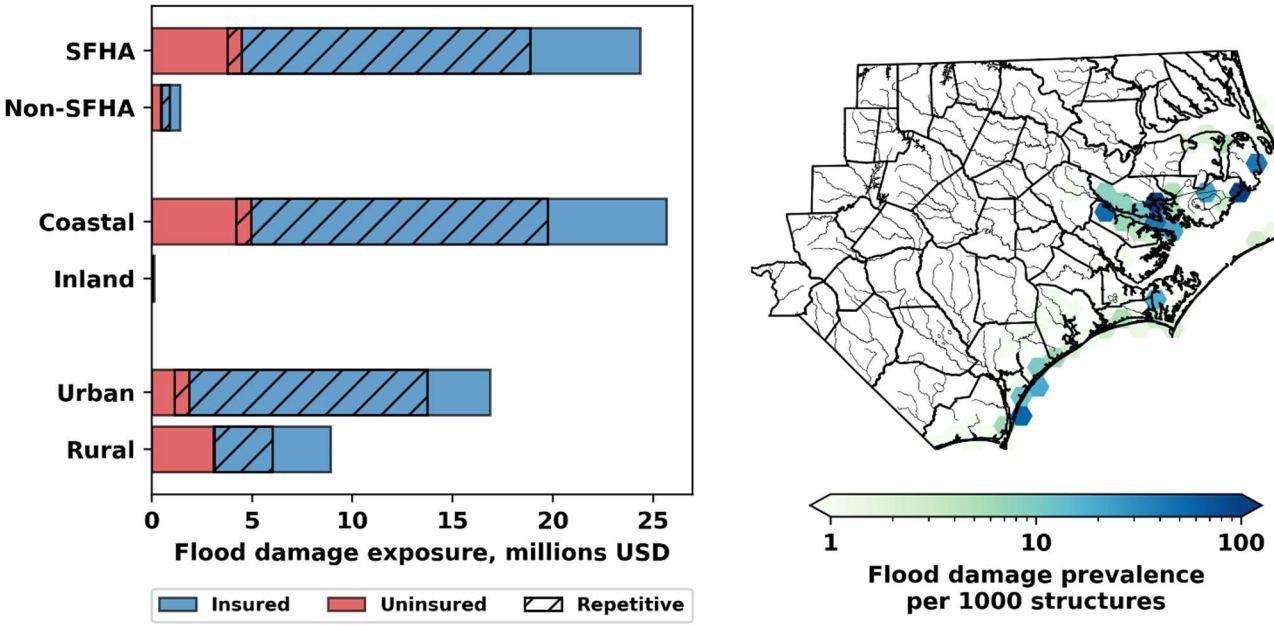

Figure S11. Prevalence and cost of flood damage during Hurricane Bonnie (1998).

The left panel depicts the aggregate cost of flood damage across comparative groups, while the right panel depicts the spatial distribution of flooded structures across a uniform 15 km hexagonal grid. Bars should only be compared within appropriate pairs (e.g., SFHA vs. non-SFHA) but not across pairs (e.g., SFHA vs. Coastal) as groups across pairs are not mutually exclusive. For display purposes, only counties that are members of the nine easternmost regional councils in North Carolina are shown.

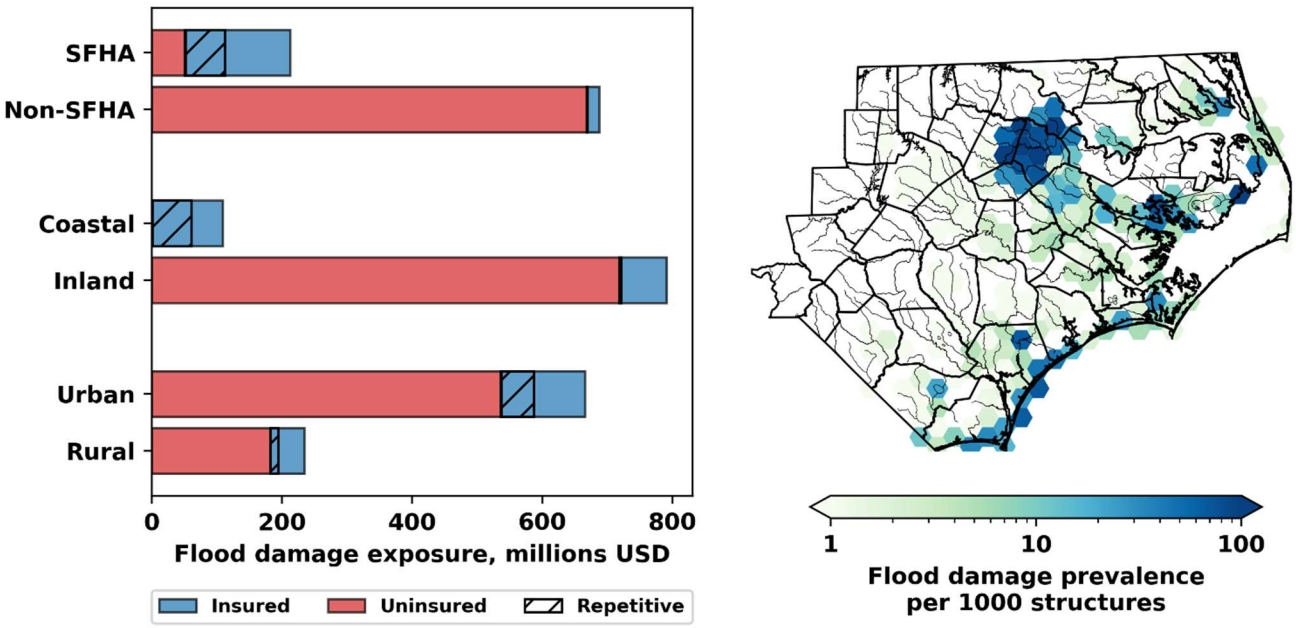

Figure S12. Prevalence and cost of flood damage during Hurricane Floyd (1999).

The left panel depicts the aggregate cost of flood damage across comparative groups, while the right panel depicts the spatial distribution of flooded structures across a uniform 15 km hexagonal grid. Bars should only be compared within appropriate pairs (e.g., SFHA vs. non-SFHA) but not across pairs (e.g., SFHA vs. Coastal) as groups across pairs are not mutually exclusive. For display purposes, only counties that are members of the nine easternmost regional councils in North Carolina are shown.

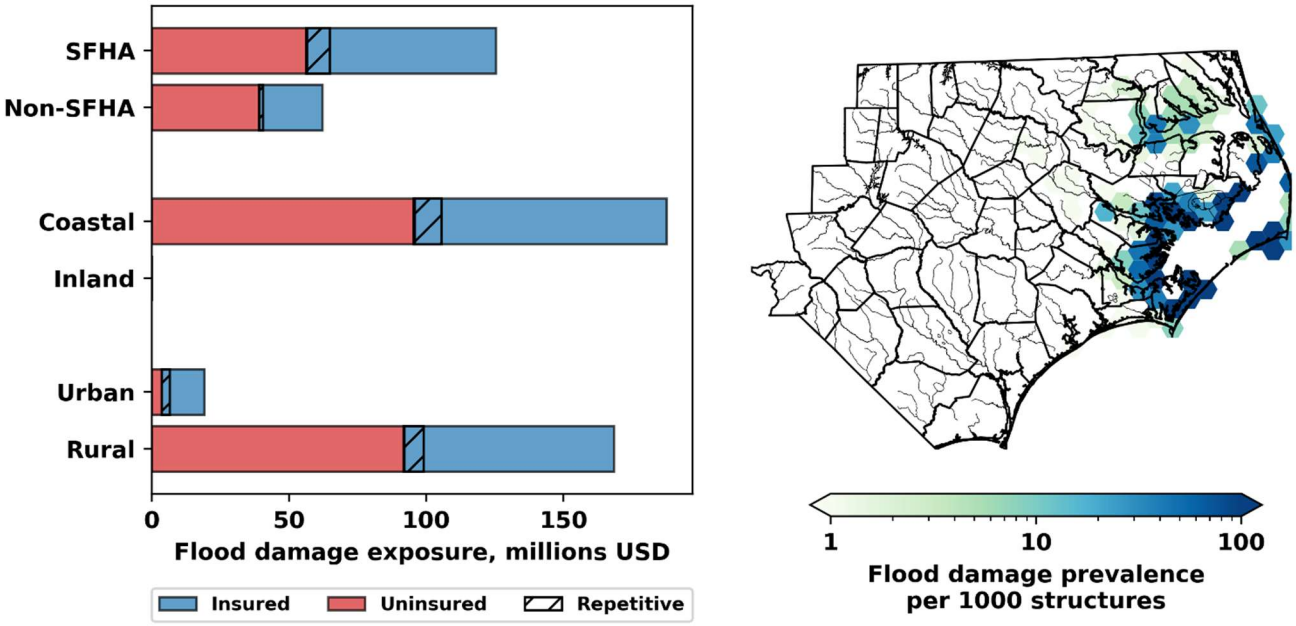

Figure S13. Prevalence and cost of flood damage during Hurricane Isabel (2003).

The left panel depicts the aggregate cost of flood damage across comparative groups, while the right panel depicts the spatial distribution of flooded structures across a uniform 15 km hexagonal grid. Bars should only be compared within appropriate pairs (e.g., SFHA vs. non-SFHA) but not across pairs (e.g., SFHA vs. Coastal) as groups across pairs are not mutually exclusive. For display purposes, only counties that are members of the nine easternmost regional councils in North Carolina are shown.

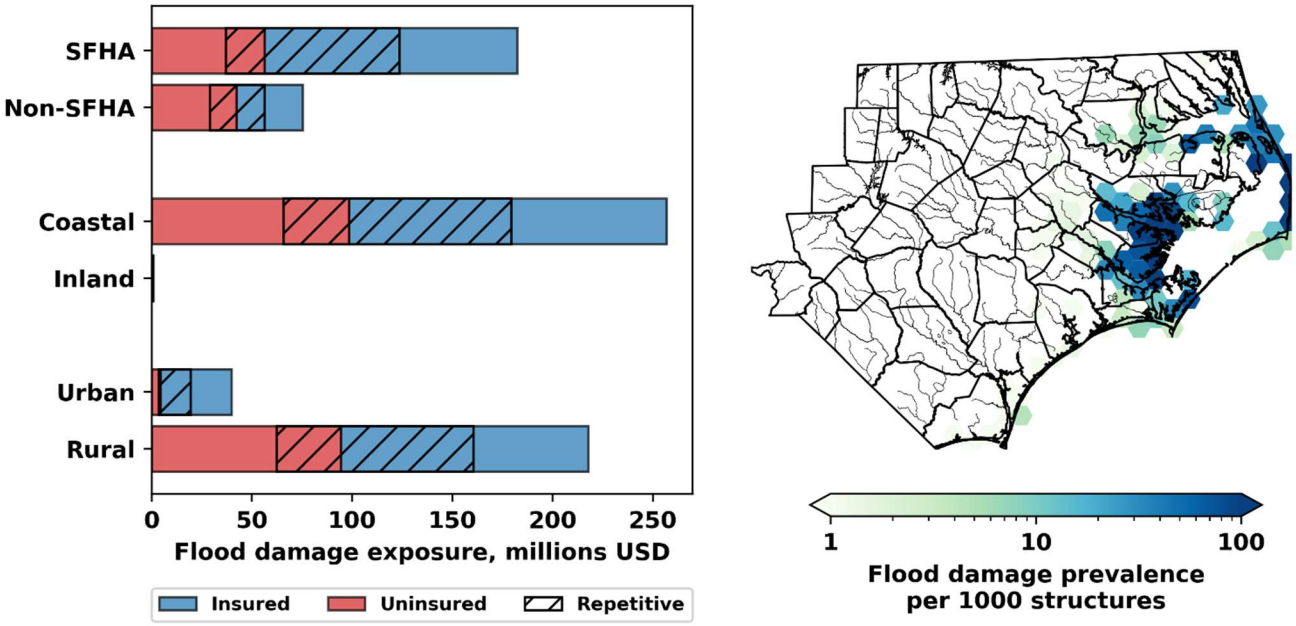

Figure S14. Prevalence and cost of flood damage during Hurricane Irene (2011).

The left panel depicts the aggregate cost of flood damage across comparative groups, while the right panel depicts the spatial distribution of flooded structures across a uniform 15 km hexagonal grid. Bars should only be compared within appropriate pairs (e.g., SFHA vs. non-SFHA) but not across pairs (e.g., SFHA vs. Coastal) as groups across pairs are not mutually exclusive. For display purposes, only counties that are members of the nine easternmost regional councils in North Carolina are shown.

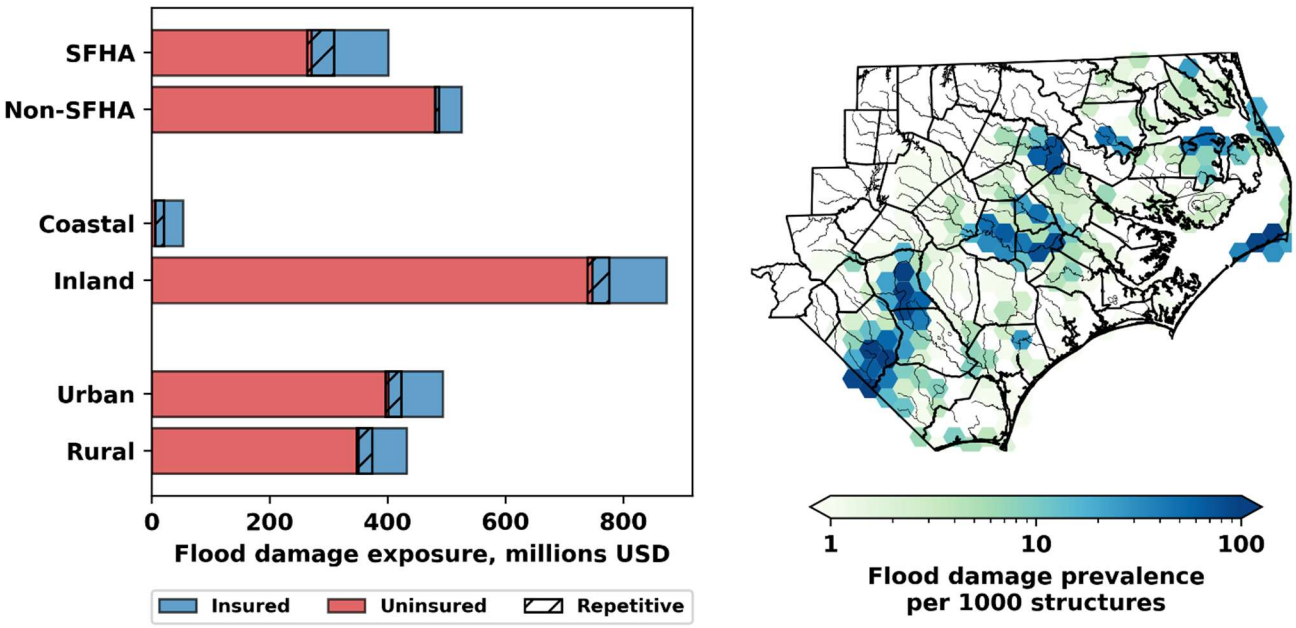

Figure S15. Prevalence and cost of flood damage during Hurricane Matthew (2016).

The left panel depicts the aggregate cost of flood damage across comparative groups, while the right panel depicts the spatial distribution of flooded structures across a uniform 15 km hexagonal grid. Bars should only be compared within appropriate pairs (e.g., SFHA vs. non-SFHA) but not across pairs (e.g., SFHA vs. Coastal) as groups across pairs are not mutually exclusive. For display purposes, only counties that are members of the nine easternmost regional councils in North Carolina are shown.

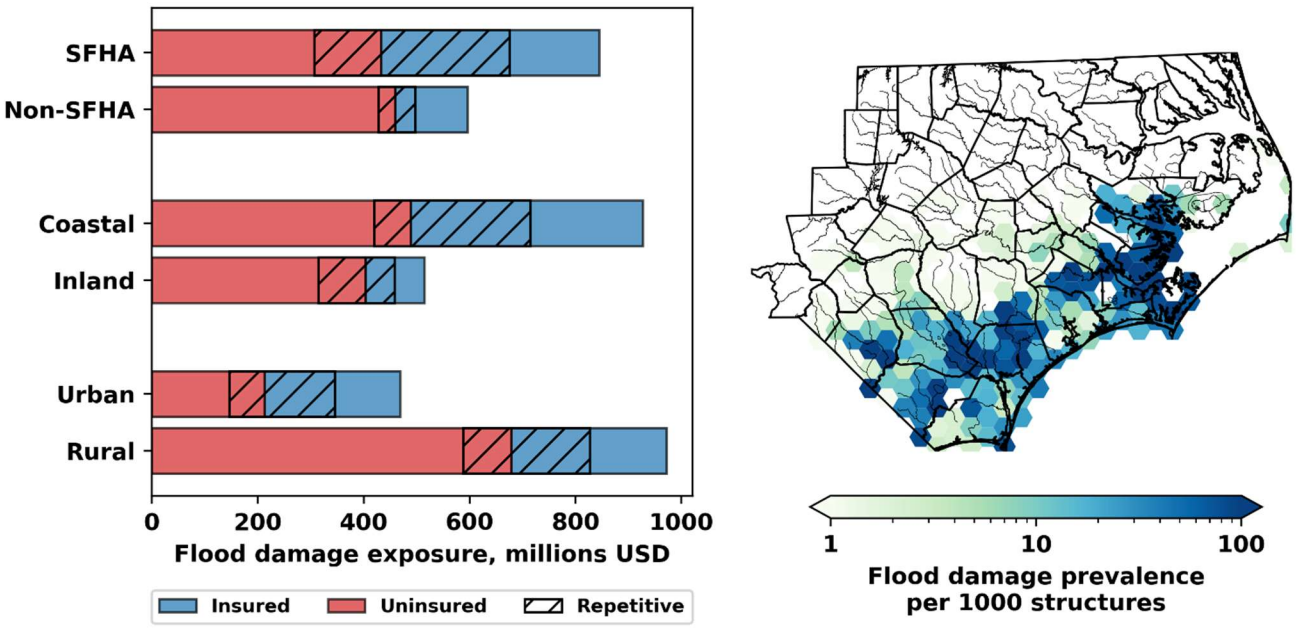

Figure S16. Prevalence and cost of flood damage during Hurricane Florence (2018).

The left panel depicts the aggregate cost of flood damage across comparative groups, while the right panel depicts the spatial distribution of flooded structures across a uniform 15 km hexagonal grid. Bars should only be compared within appropriate pairs (e.g., SFHA vs. non-SFHA) but not across pairs (e.g., SFHA vs. Coastal) as groups across pairs are not mutually exclusive. For display purposes, only counties that are members of the nine easternmost regional councils in North Carolina are shown.

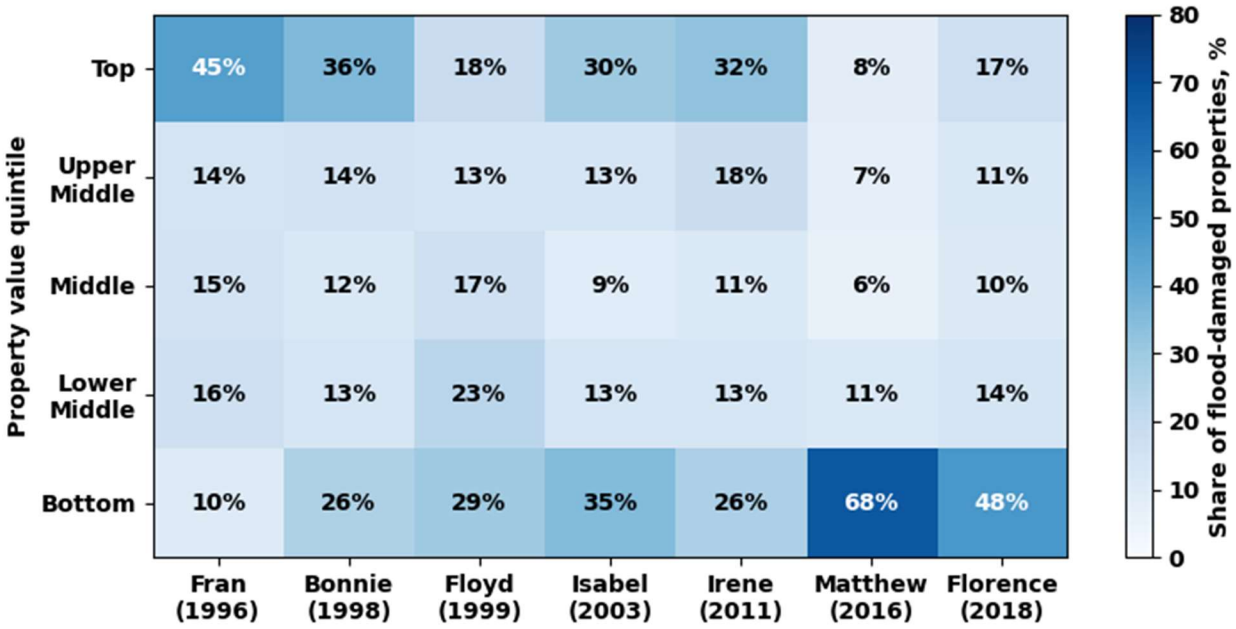

Figure S17. Proportion of flood-damaged properties in each property value quintile by event.

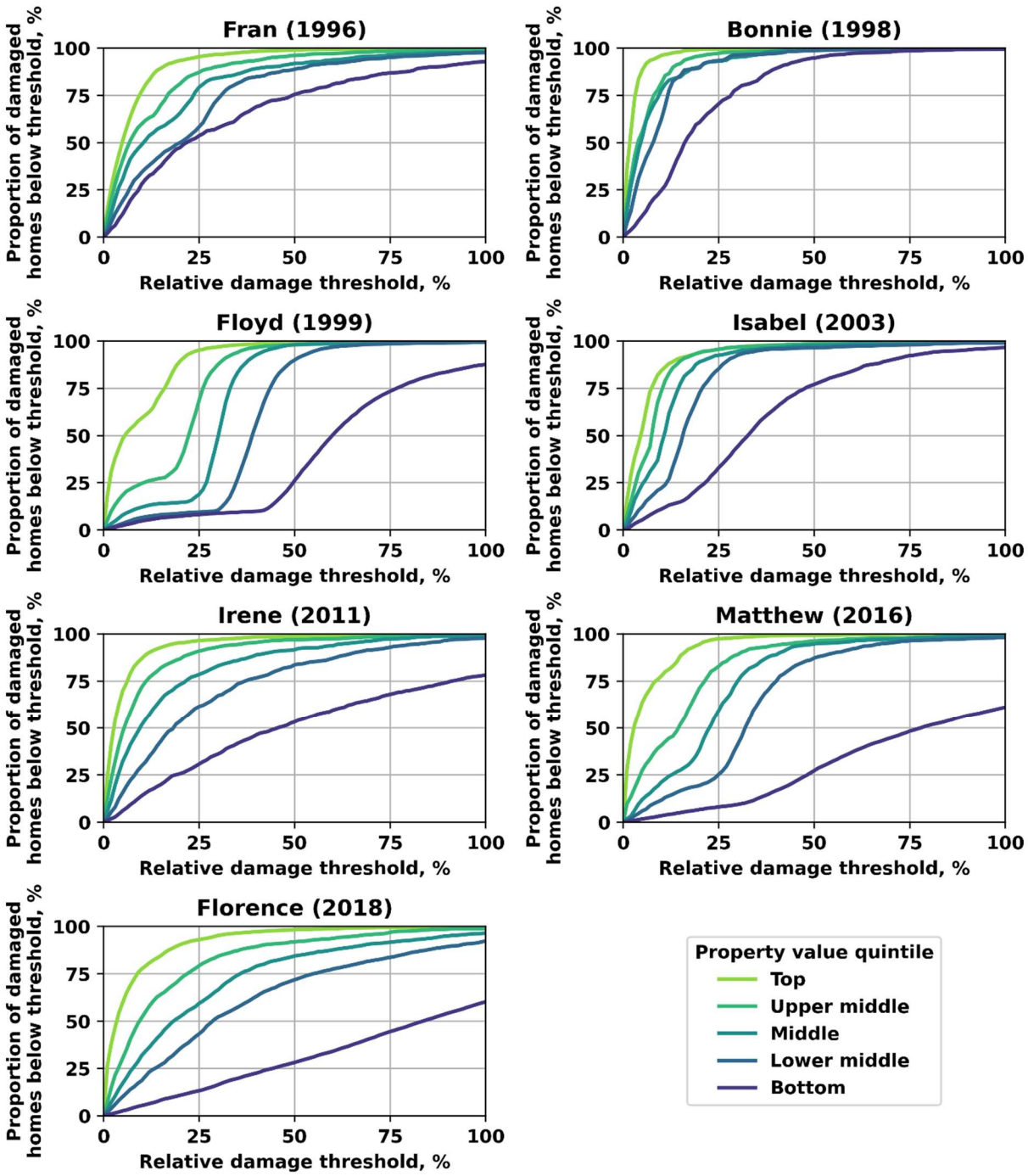

Figure S18. Cumulative distribution function of damage costs at flooded properties as a proportion of their pre-flood property value by event and property value quintile.

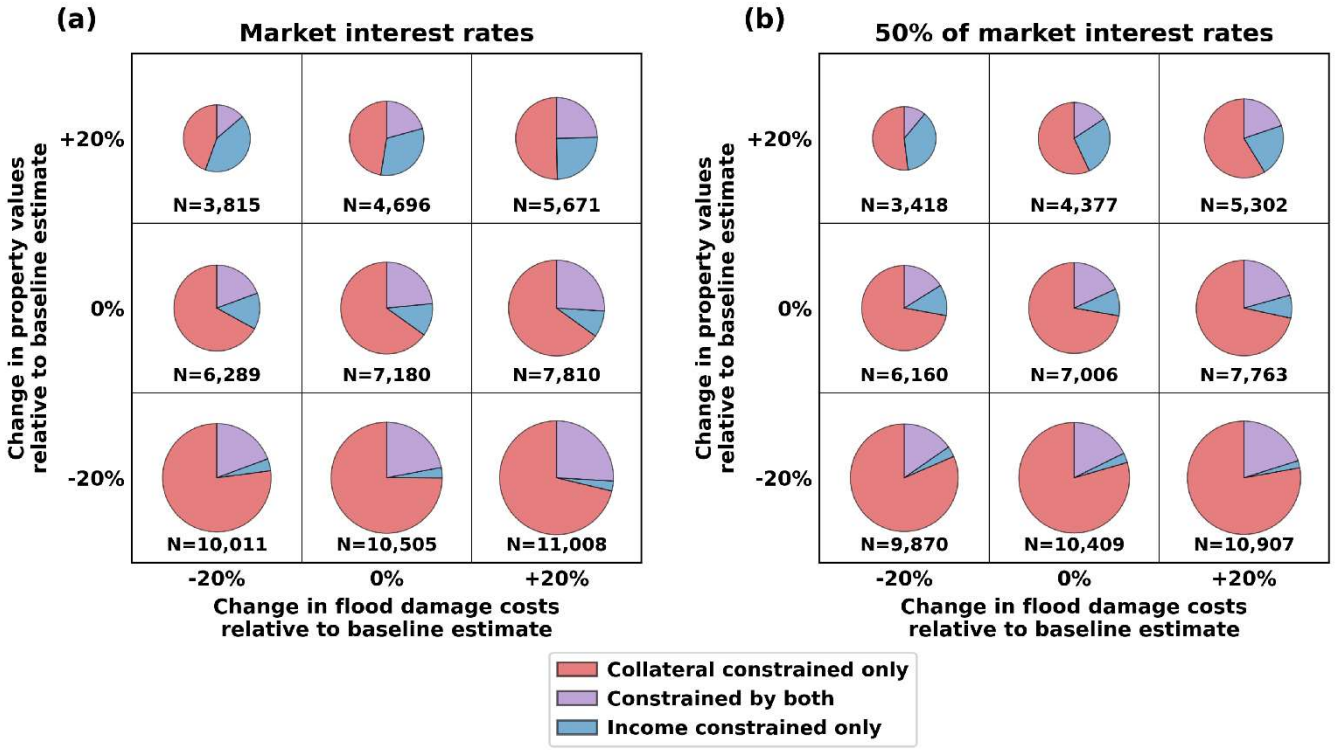

Figure S19. Scenario analysis examining alternative assumptions regarding home repair loan interest rates, property values, and flood damage costs**.**

Each panel corresponds to a different interest rate scenario: (a) one in which the interest rate on home repair loans is equivalent to the prevailing "market" rate (i.e., the average 30-year fixed rate on new mortgages); and (b) one in which the interest rate on home repair loans is equal to 50% of the prevailing market rate. Within each panel, property-level estimates of flood damage and property value are perturbed by ±20% to create a range of scenarios. Each box in the 3 × 3 plot depicts the number of borrowers projected to face flood-related credit constraints under a given scenario, as well as the share of credit constraints attributable to various drivers (e.g., insufficient collateral, insufficient income, or both in combination).

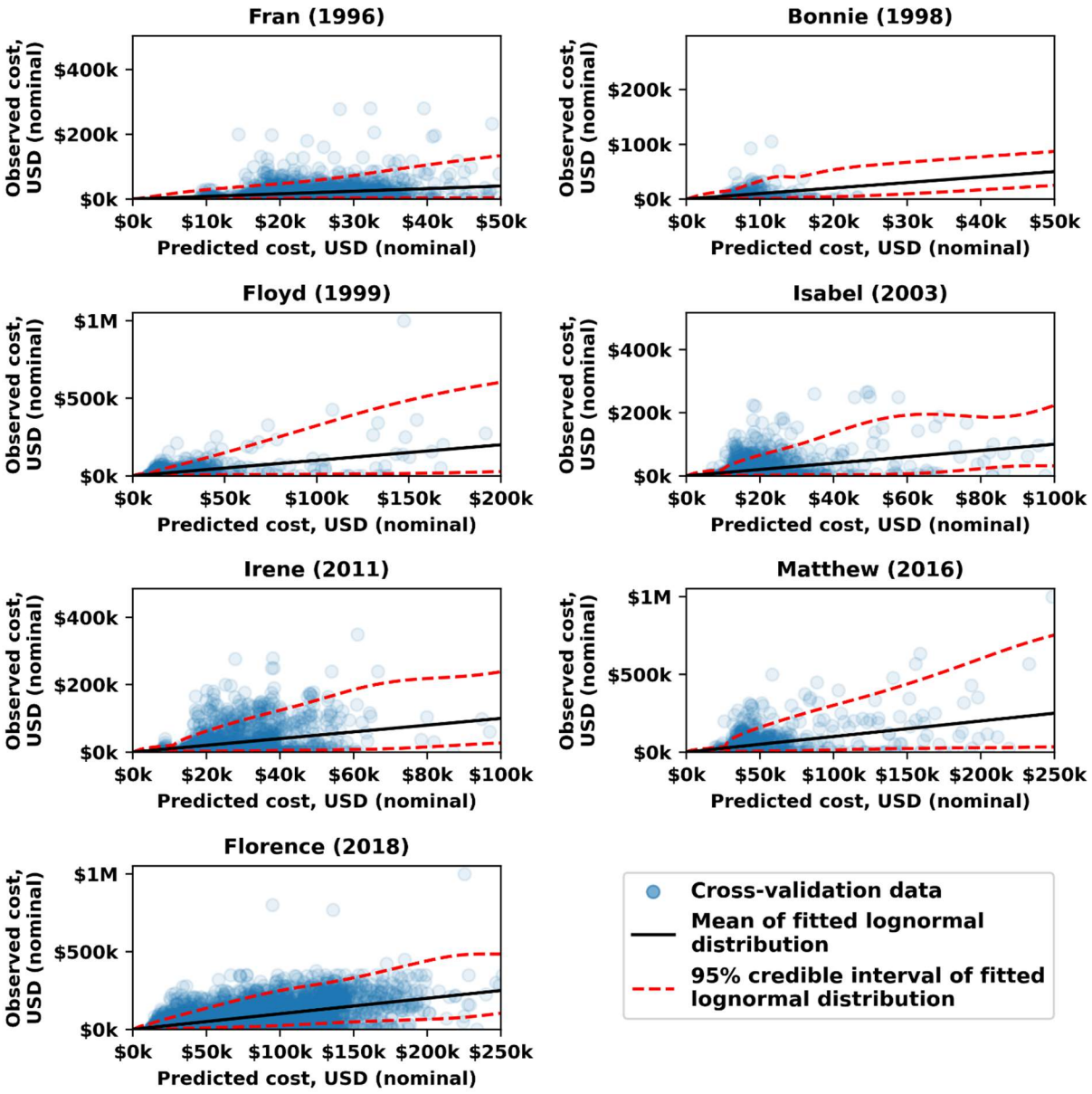

Figure S20. Uncertainty in damage costs at flooded properties.

In sensitivity analysis, damage costs were assumed to follow a lognormal distribution with a mean equal to the model-predicted cost and variance estimated from cross-validation residuals using the conditional variance estimator of Fan and Yao (1998). In the above figure, the conditional means and 95% credible intervals of the fitted lognormal distributions for each event are denoted by black and red lines respectively.

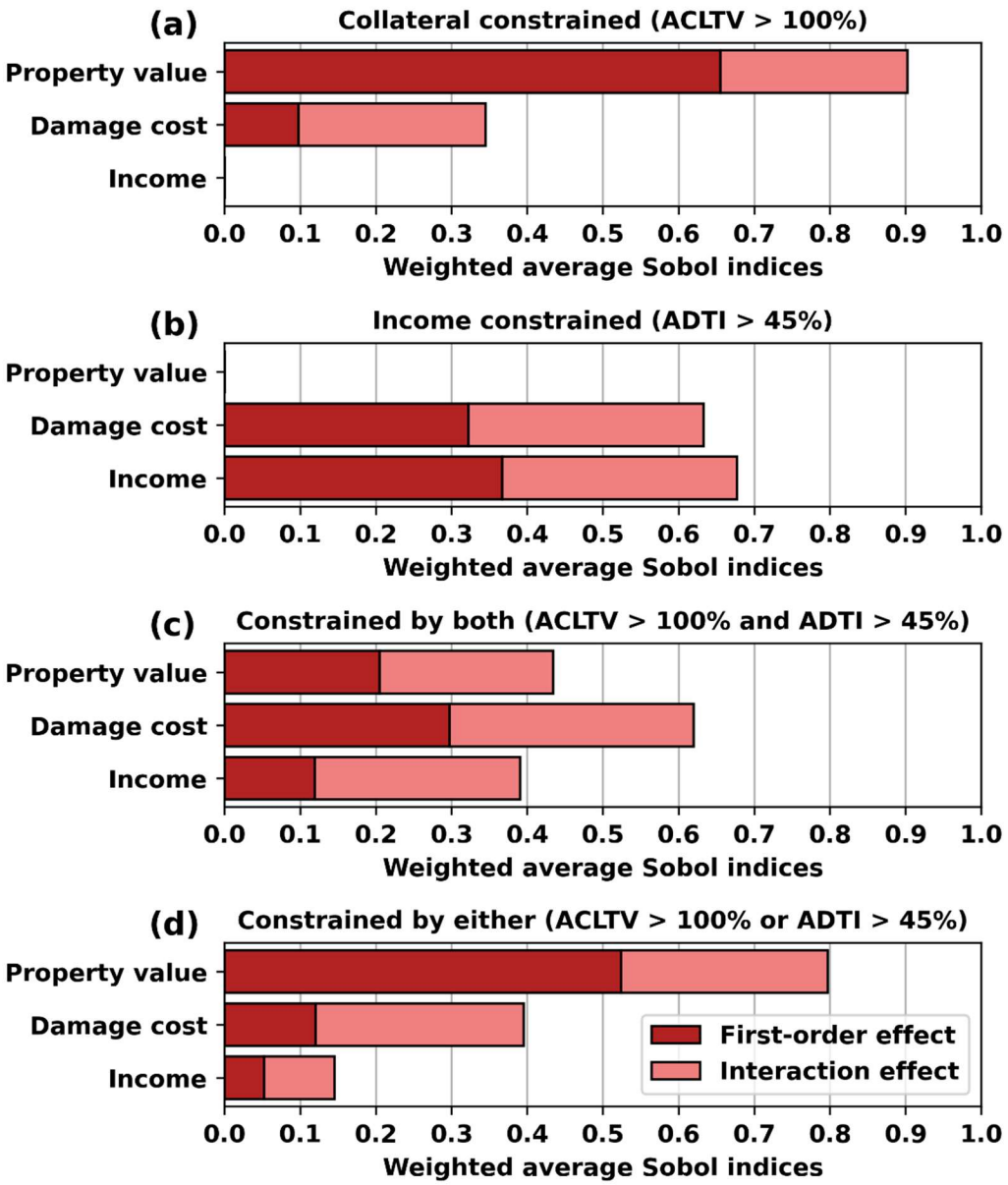

Figure S21. Weighted average Sobol' indices decomposing the relative importance of property value, damage cost, and income in determining the outcome of borrowers being credit constrained following flood exposure.

Population averages are calculated by weighing the Sobol' indices of individual borrowers by the variance in their credit constraint outcomes. Results are shown separately for (a) the outcome of being collateral constrained, (b) the outcome of being income constrained, (c) the outcome of being constrained by both measures, and (d) the outcome of being constrained by either measure. Darker bars indicate first-order effects, while lighter bars indicate interaction effects.

References

BEA: Personal Income by County, Metro, and Other Areas, https://www.bea.gov/data/income-saving/personal-income-county-metro-and-other-areas, 2023.

Chilès, J.-P. and Delfiner, P.: Geostatistics: modeling spatial uncertainty, 2. ed., Wiley, Hoboken, NJ, 699 pp., 2012.

Dynan, K., Elmendorf, D., and Sichel, D.: The Evolution of Household Income Volatility, The B.E. Journal of Economic Analysis & Policy, 12, https://doi.org/10.1515/1935-1682.3347, 2012.

Fan, J. and Yao, Q.: Efficient estimation of conditional variance functions in stochastic regression, Biometrika, 85, 645–660, https://doi.org/10.1093/biomet/85.3.645, 1998.

FEMA: OpenFEMA NFIP Redacted Policies - v2, https://www.fema.gov/openfema-data-page/fima-nfip-redacted-policies-v2, 1 August 2025.

Freddie Mac: 15-Year Fixed Rate Mortgage Average in the United States, https://fred.stlouisfed.org/series/MORTGAGE15US, 2016a.

Freddie Mac: 30-Year Fixed Rate Mortgage Average in the United States, https://fred.stlouisfed.org/series/MORTGAGE30US, 2016b.

Google Maps Platform: Geocoding API, https://developers.google.com/maps/documentation/geocoding, 2022.

Hull, J.: Options, futures, and other derivatives, Tenth Edition., Pearson, New York, NY, 868 pp., 2018.

Iaco, S. D., Myers, D. E., and Posa, D.: Space–time analysis using a general product–sum model, Statistics & Probability Letters, 52, 21–28, https://doi.org/10.1016/S0167-7152(00)00200-5, 2001.

Mathéron, G.: Les variables régionalisées et leur estimation: une application de la théorie de fonctions aléatoires aux sciences de la nature, Masson et Cie, 1965.

Saltelli, A., Annoni, P., Azzini, I., Campolongo, F., Ratto, M., and Tarantola, S.: Variance based sensitivity analysis of model output. Design and estimator for the total sensitivity index, Computer Physics Communications, 181, 259–270, https://doi.org/10.1016/j.cpc.2009.09.018, 2010.

Sobol′, I. M.: Sensitivity estimates for nonlinear mathematical models., Math. Model. Comput. Exp., 1, 407–414, 1993.

Sobol′, I. M.: Global sensitivity indices for nonlinear mathematical models and their Monte Carlo estimates, Mathematics and Computers in Simulation, 55, 271–280, https://doi.org/10.1016/S0378-4754(00)00270-6, 2001.

Virtanen, P., Gommers, R., Oliphant, T. E., Haberland, M., Reddy, T., Cournapeau, D., Burovski, E., Peterson, P., Weckesser, W., Bright, J., van der Walt, S. J., Brett, M., Wilson, J., Millman, K. J., Mayorov, N., Nelson, A. R. J., Jones, E., Kern, R., Larson, E., Carey, C. J., Polat, İ., Feng, Y., Moore, E. W., VanderPlas, J., Laxalde, D., Perktold, J., Cimrman, R., Henriksen, I., Quintero, E. A., Harris, C. R., Archibald, A. M., Ribeiro, A. H., Pedregosa, F., and van Mulbregt, P.: SciPy 1.0: fundamental algorithms for scientific computing in Python, Nat Methods, 17, 261–272, https://doi.org/10.1038/s41592-019-0686-2, 2020.